This manuscript has been submitted for publication in *Nature Communications*. It has not undergone peer review yet. Subsequent versions of the manuscript may have slightly different content. If accepted, the final version of this manuscript will be available via the "Peer-reviewed Publication DOI" link on the EarthArXiv webpage.
Please feel free to contact us; we welcome feedback.

Decrease in air-sea CO_2 fluxes caused by persistent marine heatwaves

Authors: A. Mignot[1*], K. von Schuckmann[1], F. Gasparin[1], S., van Gennip[1], Peter Landschützer[2], C. Perruche[1], J. Lamouroux[1], Tristan Amm[1]

Affiliations :

[1]Mercator Océan, Ramonville Saint-Agne, France.

[2]Max Planck Institute for Meteorology, Hamburg, Germany.

[*] Correspondence to: mignot@mercator-ocean.fr

Abstract

Regional processes play a key role in the global carbon budget. Major ocean carbon uptake at mid-latitudes counteracts carbon release in the tropics, which is modulated by episodes of marine heatwaves (MHWs). Yet, we lack essential knowledge on persistent MHWs (PMHWs), and their effect on the carbon sensitive areas. Here, based on a 1985-2017 joint analysis of reconstructions, ocean reanalysis, *in situ* and satellite data, we show that PMHWs occur in major carbon uptake and release areas. Air-sea CO_2 flux changes from PMHWs are strongest in the Pacific Ocean with a 35 +/- 2 % reduction in CO_2 release in the tropics linked to ENSO, and a reduction in CO_2 uptake of 28 +/- 9 % in the North Pacific. These results provide new insights into the interplay of extreme variability and a critical regulating ocean ecosystem service, and pave the way for future investigations on its evolution under climate change.

1. Introduction

Extreme events driven by unusually high-water temperature are ubiquitous in the global ocean. They can last from weeks to years, span from local to interbasin scale, and reach depths of several hundreds of meters[1–3]. These so-called marine heatwaves (MHWs) occur due to either coupled air-sea interactions[4–7], ocean internal processes such as circulation changes – horizontal and/or vertical[8], and are sometimes linked to large climate modes such as the El Niño-Southern Oscillation (ENSO)[5]. Over the past 35 years, MHWs have doubled in frequency, become longer-lasting, more intense and more extensive[9–11]; an amplification very likely due to long-term anthropogenic change[1,9,10,12,13].

Strong and long-lasting MHWs have been reported at different locations in the global ocean[3,5]. These include the 2013/2015 Northeast Pacific 'warm blob'[4,14], the 1997/1998 El Niño[15], the 2015/2016 Tasman Sea[16] or the 2012 Northwest Atlantic[17,18]. The duration of these major events ranges from several months up to 2 years, they are associated with dramatic increase in sea surface temperature of up to 10°C, and they can extend over large regions, reaching sometimes ~ 10M km^2 [5]. Due to their extreme nature, MHWs, and in particular the strong, persistent ones, pose a fundamental challenge for societies as they have devastating impacts on the marine ecosystem and their services[1,11,19].

Overall, the ocean acts as a net sink for atmospheric CO_2 and is absorbing about a ¼ of CO_2 anthropogenic emissions[20] (2.6+/-0.6 PgC/yr over the 2009-2018 period), thereby mitigating global warming. Carbon entering the ocean is then redistributed horizontally over large distances and into deep ocean layers where it is then stored for long time scales[21–23]. The magnitude and direction of air-sea CO_2 fluxes (F_{CO2}) vary widely in space and time, and depend on hydrographic conditions, the ocean circulation system, biological production and air-sea interactions. As a result, major carbon uptake areas are located at mid-latitudes, whereas carbon release takes place predominantly in upwelling areas such as the tropical ocean[24–26] (Fig. 1a).

Persistent MHWs linked to ENSO[5] affect the Tropical Pacific carbon source region and lead to significant reduction in CO_2 outgassing[27–31]. However, we lack essential knowledge about how these major MHWs events affect other oceanic carbon sources and sink regions. Here we investigate the interplay and the impact of strong and long-lasting MHWs on the air-sea CO_2 flux at the global scale. The study is built on a combined use of reconstructions from 1985 to 2017, direct measurements, remote sensing data and an ocean reanalysis. We first present the regions where particularly strong and long-lasting MHWs most frequently occur. We then quantify the impact of these extreme ocean events on oceanic carbon sink and sources areas. We further examine the interaction between these extreme ocean events and one critical oceanic carbon sink region in the North Pacific Ocean. Finally, we discuss these results with existing knowledge on the mechanisms in the Tropical Pacific region to obtain a large-scale view of the prevailing mechanisms driving coupled changes between the regulating ocean ecosystem service and extreme variability.

2. Results

a. Persistent marine heatwaves occurrence and oceanic carbon source and sink areas

In the Tropical Pacific, strong and long-lasting MHWs (hereinafter denoted persistent marine heatwaves, PMHWs), have a higher impact on ocean CO_2 fluxes than short-lived and less intense MHWs[30]. We propose specific new criteria to identify such PMHWs at the global scale based on the duration and the mean Sea Surface Temperature (SST) anomaly during a MHW. We first detect all MHWs that occurred from 1985 to 2017 by applying a standard MHW detection algorithm[2] to NOAA gridded SST data derived from AVHRR sensor[32,33] (see method section). The detection algorithm provides several metrics that describe MHWs, including the duration and the mean SST anomaly. Using these two metrics, we define PMHWs as MHWs whose duration and mean SST anomaly are greater than the 95th percentile of their historical distribution, i.e., duration > 38 days and mean SST anomaly > 2.3 degrees Celsius. Finally, we focus on the regions where PMHWs have appeared several times over the past three decades, and that represent a recurring threat for the global ocean carbon sink, similar to El Niño events in the Tropical Pacific. To do so, we only consider the points where PMHWs have re-occurred at least three times during the 1985-2017 period (grey points in Fig.1a) -- which correspond to 25 % of all grid points that have experienced at least one PMHW.

Globally, PMHWs most frequently occur in the largest oceanic carbon source and sink areas. Critical sink regions are located at mid-latitudes in the Northern and Southern Hemispheres (plain contours in Figure 1a), while ocean carbon outgassing mainly occurs in upwelling regions such as the Tropical Pacific (dashed contours in Fig. 1a) and correspond to regions where climatological F_{CO2} is greater/lower (sinks/sources) than 1/-1 molC/m^2/year (plain and dashed contours in Fig. 1a), as proposed by Takahashi et al.[34]. The climatological F_{CO2} values are illustrated for the 1985-2017 period using the observation-based Copernicus

Marine Environment Monitoring Service (hereafter denoted CMEMS) product[35] (see method section). Unexpectedly, we find that the regions with a strong occurrence of PMHWs (grey points) are mainly located in the largest oceanic sources and sinks areas in the global ocean, and particularly in the Pacific Ocean (Fig. 1a).

Amongst the largest oceanic carbon sinks and sources where PMHWs most frequently occur, the North Pacific and the Tropical Pacific are the most impacted, and both areas suffer from a significant reduction in CO_2 uptake (28 +/- 9 %) and outgassing (35 +/-2%) during PMHWs respectively. PMHWs impact on F_{CO2} is quantified using an ensemble of four observation-based products of F_{CO2} from 1985 to 2017 (see method section). In contrast, in the North Atlantic and the Southern Ocean carbon sinks, the impact of PMHWs on F_{CO2} is close to 0 and negligible over the study period. The impact of PMHWs on F_{CO2} appears thus to be the most important in the Tropical and North Pacific, which is of considerable concern given their contributions to the global ocean carbon cycle[24–26] .

b. Persistent marine heatwaves and the North Pacific carbon sink

We use a state-of-the-art ocean biogeochemical reanalysis[36] (see supplementary information), validated against F_{CO2} reconstructions and *in situ* observations from BGC-Argo floats[37,38], to understand the interaction between PMHWs and F_{CO2} in the North Pacific from 2009 to 2017. Note that, the calculations relative to the 2009-2017 period are performed on those North Pacific regions where PMHWs have re-occurred several times since 1985, i.e. the SST grid points that have experimented at least 3 PMHWS from 1985 to 2017. The exchange of CO_2 between the ocean and the atmosphere is driven by six variables[39]: wind, upper-ocean temperature, salinity, dissolved inorganic carbon (DIC) and alkalinity (ALK) as well as the atmospheric partial pressure of CO_2. As observation-based products of F_{CO2} do not include all these variables, the reanalysis becomes essential to pursue the analysis. The BGC reanalysis combines ocean circulation and biogeochemistry models together with *in situ* and satellite observations to provide a high degree of bio-physical realism[40]. The reanalysis skill is validated against the ensemble of observation-based products over the 2009-2017 period and *in situ* observations from an array of BGC-Argo floats during the 2013/2015 ‘warm blob’ PMHW (see supplementary Information). The reanalysis shows good agreement with the observation-based products in estimating F_{CO2} anomalies due to PMHWs in the North Pacific. The reanalysis also agrees well with the float observations in reproducing anomalies in the four oceanic drivers known to control F_{CO2} (temperature, salinity, DIC and ALK) during the 'warm blob'.

During PMHW events, the reduction in F_{CO2} is the result of higher-than-usual temperature and negative DIC anomalies. We calculate a first-order Taylor series expansion of F_{CO2} anomalies to determine the contribution of the four oceanic drivers[27,41,42] (see method section). The Taylor decomposition (Fig. 2a) reveals that the negative F_{CO2} anomalies during PMHWs in the North Pacific mainly result from the contribution of temperature (-1.43 +/- 0.02 molC/m2/yr), DIC anomalies (0.81 +/- 0.01 molC/m2/yr) and to a lesser extent ALK anomalies (0.23 +/- 0.01 molC/m2/yr) . The contribution from salinity, wind and the atmospheric partial pressure of CO_2 anomalies are small, and can be considered negligible. Sea surface warming during PMHWs reduces the solubility of CO_2 in the ocean resulting in a reduced uptake of CO_2. In contrast, the decrease in DIC associated with a small increase in ALK (Fig. S3) enhances the uptake of CO_2 and as such counterbalances the thermal effect to the extent that the final F_{CO2} anomaly is ~4 times smaller than it would have been from the thermal effect alone.

Next, we investigate the mechanisms leading to negative DIC anomalies. We examine the processes that drive the rate of change (tendency or trend) of DIC anomalies during PMHWs over the 2009-2017 period. The budget (or forcing) terms in the DIC trend equation consist of: horizontal and vertical advection, vertical diffusion, air-sea flux of CO_2, biological activity, dilution and concentration due to freshwater fluxes and a residual term (see method section). To highlight the contribution from each process to the DIC anomalies trend, we follow the method of Doney et al.[27] and examine the slope through linear regression of each forcing term to the DIC anomalies trends (Fig. 2b) (we verify that the intercept is approximately 0 because the average of the forcing term anomalies is null). A slope close to 1 indicates that a particular forcing term produces in-phase anomalies of comparable magnitude to DIC anomalies trend. In contrast, a slope near zero indicates that the term is not important, and a negative slope that the term produces out of phase anomalies.

Horizontal advection is the main driver for DIC anomalies. The linear regression slope of horizontal advection on DIC anomalies trends is the largest (0.70 +/-0.02 (unitless)) whereas the slopes of the other forcing terms are much smaller (<0.16 (unitless) for vertical diffusion anomalies and lower than 0.06 (unitless) for all the other terms). Furthermore and consistently with Ayers and Lozier[43] and Gruber et al[22], the reanalysis shows that, on average, there is a net horizontal divergence of DIC in the North Pacific carbon sink region (data not shown). The reanalysis suggests that the lateral removal of DIC is further accentuated during PMHWs, causing a decrease in DIC. Changes in horizontal advection have already been observed during the 2013/2015 PMHW 'warm blob'[4] in the Northeast Pacific but it is not clear how changes in horizontal advection are related to PMHWs at the scale of the North Pacific carbon sink region. Given the importance of the horizontal transport of DIC in mitigating the impact of PMHWs on the uptake of CO_2, we propose that studies should address how PMHWs and ocean circulation are interconnected in this region.

3. Discussion

We show that PMHWs (> 38 days and > 2.3°C anomalies as defined in this study) most frequently occur in oceanic regions of major importance for the global carbon cycle: the Tropical Pacific carbon source area, and the carbon sink regions of the North Pacific, the North Atlantic and the Southern Ocean. However, over the study period 1985-2017, PMHWs impact air-sea exchange of CO_2 only in the Pacific carbon sensitive areas, and in ways that attenuates the ocean's role as source and sink. The processes of this interplay are provided in the schematic of Fig. 3.

In the North Pacific carbon sink, PMHW events cause a reduction in the CO_2 sink as a result of the net effect of two competing mechanisms: extreme higher-than-average temperature and anomalous DIC advection. The former causes a reduction in the solubility of CO_2 in ocean water, thereby reducing the ocean uptake of CO_2 whereas the latter increases the ocean CO_2 uptake – through decreased levels of DIC driven by horizontal advection – and as such attenuates the impact of the thermal effect. Overall, the thermal effect dominates the advection effect in our study, leading to a net reduction in air-to-sea CO_2 flux during a PMHW event of about 28 +/- 9 % (Fig. 3a).

In the Tropical Pacific where carbon release takes place, the CO_2 outgassing is significantly attenuated during PMHWs with a reduction in CO_2 release from the ocean to the atmosphere of about 35 +/- 2 %. In this region, PMHWs are associated with ENSO[5] and previous studies have investigated the mechanisms explaining this change, which is mainly driven by a change in the vertical ocean circulation[27–31]. During PMHWs (Fig. 3b), eastward propagating Kelvin waves that depress the thermocline in the east together with a concurrent weakening of easterly winds, and the extension of the western Pacific warm pool to the east, reduce the upwelling of DIC leading to a net decrease in sea-to-air CO_2 flux.

The results in the North Pacific carbon sink complete previous studies of ENSO-related PMHWs in the Tropical Pacific, and together with the new results obtained in this study thus provide a comprehensive view on the interplay between PMHWs and carbon sensitive areas in the Pacific Ocean as illustrated in Fig. 3.

The attenuation in F_{CO2} due to PMHWs has increased during the 1985-2017 period in the North Pacific whilst remaining stable in the Tropical Pacific (Fig. 4). Similarly, PMHWs have also increased in intensity in the North Pacific over the last decades, while their strength remains similar in the Tropics (Fig. S5). Based on the results of our process study, we can develop the hypothesis that the reported increase in the intensity of PMHWs has potentially amplified the outgassing of CO_2 over the 1985-2017 period, and that the competing mechanism, i.e., anomalous advection of DIC, was unable to counter-interact the thermal effect over this time scale. However, we cannot test such hypothesis as it would require a decomposition of F_{CO2} and DIC budgets from 1985 to 2017, the latter being currently not estimated by the reanalysis over this period. MHWs are projected to become stronger, more frequent and longer lasting in a warming climate[1,9,12,13]. Therefore, it is crucial to understand how PMHWs and F_{CO2} interact over long time scale if we want to further unravel the evolution of the oceanic carbon cycle under climate change.

4. Methods

a. Observation-based products of F_{CO2}

In this study, we use an ensemble of four observation-based products to quantify the impact of PMHWs on F_{CO2} in the three largest oceanic carbon sink and the largest oceanic carbon source in the Tropical Pacific from 1985 to 2017. Here, we provide a brief outline of the chosen products. More detail can be found in their respective publications.

The first observation-based product, from the Max Plank Institute for Meteorology (hereinafter denoted MPI)[44,45], is based on a self-organizing map–feed-forward network that reconstructs the sea surface partial pressure of CO_2 ($spCO_2$) from various environmental predictor data. In a first step, the ocean is divided into biogeochemical regions of similar $spCO_2$ properties (making use of a $spCO_2$ climatology) and in a second step the non-linear relationship between auxiliary driver data and sparse observations is reconstructed to fill measurement gaps. The period of analysis is from 1982 to 2019 at monthly intervals and with a spatial resolution of 1° × 1°. It is based on a collection of ship and mooring $spCO_2$ measurements assembled by the Surface Ocean CO_2 Atlas (SOCAT) version 2020[46–49] .

The second observation-based product, from Copernicus Marine Environment Service (hereinafter denoted CMEMS)[35], is from an ensemble-based forward feed neural network that reconstruct change in $spCO_2$ from environmental predictor data. The period of analysis is from 1985 to 2018 at monthly intervals and with a spatial resolution of 1° × 1°. It is based on a collection of ship and mooring $spCO_2$ measurements assembled by the Surface Ocean CO_2 Atlas (SOCAT) version 2019[46–49].

The third observation-based product, from the Council for Scientific and Industrial Research (hereinafter denoted CSIR)[50], is from a machine-learning ensemble average of six two-step clustering-regression models that reconstruct change in $spCO_2$ from environmental predictor data. The period of analysis is from 1982 to 2019 at monthly intervals and with a spatial resolution of 1° × 1°. It is based on a collection of ship and mooring spCO2 measurements assembled by the Surface Ocean CO_2 Atlas (SOCAT) version 2019[46–49].

The fourth observation-based product, from the Max Plank Institute for Biogeochemistry (hereinafter denoted Jena)[51], is from an observation-driven ocean mixed-layer scheme that reconstruct change in $spCO_2$ by fitting a data-driven diagnostic model of ocean mixed-layer biogeochemistry to surface-ocean CO_2 partial pressure data from the SOCAT version 2019[46–49]. The period of analysis is from 1982 to 2017 at daily intervals and with a spatial resolution of 4° × 5°. The daily fields were averaged into monthly fields.

Finally, to evaluate the skill of the BGC reanalysis in estimating F_{CO2} anomalies associated with PMHWs in the North Pacific carbon sink , we use an additional observation-based product, from the Japan Meteorology Agency (hereinafter denoted JMA)[52], which is excluded from the $spCO_2$ ensemble as its period of analysis is shorter than the previously listed products, i.e. from 1990 to 2018. This product is based on multiple linear regressions that reconstruct change in $spCO_2$ from a set of environmental drivers. The temporal resolution is monthly intervals and with a spatial resolution of 1° × 1°. It is based on a collection of ship and mooring $spCO_2$ measurements assembled by the Surface Ocean CO_2 Atlas (SOCAT) version 2019 [46–49].

b. Estimates of air-to-sea fluxes of CO_2 from $spCO_2$ data

In the five observation-based products and the BGC reanalysis, air-to-sea fluxes of CO_2 are generated from $spCO_2$ data using the gas exchange formulation[53],

$$F_{CO2}=k\alpha(pCO_{2atm} - spCO_2), \qquad (1)$$

where α is the CO_2 solubility in seawater, k, a gas transfer coefficient , pCO_{2atm} is the atmospheric partial pressure of CO_2 and $spCO_2$ is the sea surface partial pressure of CO_2. Here, positive values of F_{CO2} indicate uptake of CO_2 from the atmosphere to the ocean, while negative values indicate outgassing of CO_2 from the ocean to the atmosphere. Each product performs their own calculation of the fluxes and the methods are described in the respective publications

c. Calculation of 2009-2017 monthly anomalies

In the reanalysis and the observation-based products, monthly anomalies (hereinafter denoted with a prime) are computed by removing a climatological value (hereinafter denoted with an overbar). The climatological value corresponds to the sum of a long-term linear trend and a monthly mean value. The monthly mean values are computed from the detrend monthly data.

d. Calculation of 1985-2017 percent F_{CO2} anomalies

The percent F_{CO2} anomalies during PMHWs and for the 1985-2017 period correspond to the monthly F_{CO2} anomalies divided by the monthly F_{CO2} climatological values. The anomalies and climatological values were computed following the method detailed previously (subsection c), with the exception that monthly mean values were only computed from the detrend monthly data over the 1985-1995 period. During this decade, the number of PMHWs per year, and globally, were the lowest of the 1985-2017 period (see Fig. S4). By calculating the anomalies relative to this "reference" decade, we make sure that the percent F_{CO2} anomalies represent a change with respect to oceanic conditions not impacted by PMHWs.

In Fig. 1b, we represent, in each carbon sink/source, an ensemble of four 1985-2017 trimmed mean percent F_{CO2} anomalies derived from the observation-based products. We use the trimmed mean instead of the mean because it is a robust estimator of central tendency and provides a better estimation of the location of the bulk of the data than the mean when the distribution is asymmetric, which is the case here. More precisely, we use a 5% trimmed mean, i.e., the lowest 5 % and the highest 5 % of the data are excluded .

Finally, in the main text, we report the ensemble of the four 1985-2017 trimmed average percent F_{CO2} anomalies with the ensemble mean +/- ensemble standard-deviation; the latter providing an estimate of the uncertainty. This is a reasonable assumption considering that systematic errors in the observation-based products of F_{CO2} are much more smaller than their random errors[50], so that the full uncertainty can be approximated by the ensemble spread.

e. Taylor expansion of F_{CO2} anomalies

To determine the driving mechanisms causing F_{CO2} anomalies during PMHWs in the North Pacific carbon sink, we calculate a first-order Taylor series expansion of F_{CO2} anomalies in terms of its driving parameters (i.e., wind, upper ocean temperature, salinity, dissolved inorganic carbon (DIC), alkalinity (ALK) and the atmospheric partial pressure of CO_2)[27,41].

First, we performed the linear Taylor decomposition of Eq. (1) :

$$F_{CO2}' \approx (k\alpha)'\overline{(pCO_{2atm} - spCO_2)} + \overline{(k\alpha)}pCO_{2atm}' - \overline{(k\alpha)}spCO_2'. \quad (2)$$

The right-hand-side terms represent the contribution to F_{CO2}' of gas transfer and solubility anomalies, atmospheric pCO_2 anomalies and $spCO_2$ anomalies. Note that the temperature dependence of k and α cancel each other, and $(k\alpha)'$ is mainly driven by variations in wind speed[27,41].

The $spCO_2$ anomalies are further decomposed into contributions from sea surface temperature anomalies (SST'), sea surface dissolved inorganic carbon anomalies (SDIC'), sea surface alkalinity anomalies (SALK') and sea surface salinity anomalies (SSS'), neglecting the second-order terms[27,41,42,54]:

$$spCO_2{}' \approx \frac{\partial spCO_2}{\partial SDIC} SDIC' + \frac{\partial spCO_2}{\partial SALK} SALK' + \frac{\partial spCO_2}{\partial SST} SST' + \frac{\partial spCO_2}{\partial SSS} SSS'. \quad (3)$$

Substituting Eq. (3) into Eq. (2) gives the contributions of all parameters to F_{CO2}' in a single expression:

$$F_{CO2}{}' \approx (k\alpha)'\overline{(pCO_{2atm} - spCO_2)} + \overline{(k\alpha)} pCO_{2atm}{}' - \overline{(k\alpha)} \left(\frac{\partial spCO_2}{\partial SSDIC} SDIC' + \frac{\partial spCO_2}{\partial SSALK} SALK' + \frac{\partial spCO_2}{\partial SST} SST' + \frac{\partial spCO_2}{\partial SSS} SSS' \right). \quad (4)$$

Here, the sea surface quantities correspond to the quantities at the first level of the ocean reanalysis estimates (z ~ - 0.50 m). Following Doney et al.[27], the partial derivatives in Eq. (4) were computed off-line at each grid point, taking SDIC as an example, as:

$$\frac{\partial spCO_2}{\partial SDIC} \approx \frac{spCO_2(SDIC, \overline{SAlk}, \overline{SST}, \overline{SSS}) - spCO_2(\overline{SDIC}, \overline{SALK}, \overline{SST}, \overline{SSS})}{SDIC'} . \quad (5)$$

where spCO2 values are calculated using the seacarb program for R (https://CRAN.R-project.org/package=seacarb).

f. DIC anomalies budget

In our study, we show that DIC anomalies play a significant role in controlling F_{CO2} anomalies during PMHWs. We therefore conduct a DIC anomalies budget to elucidate what processes controlled DIC anomalies.

In the ocean reanalysis, the changes in DIC concentration with time are described by the following equation:

$$\frac{\partial DIC}{\partial t} = ADV_H + ADV_z + DIFF_z + SBC + F_{CO2} + B + r. \qquad (6)$$

The right-hand-side terms represent the horizontal and vertical advection of DIC, the vertical diffusion of DIC, freshwater fluxes that dilute or concentrate DIC, biological activity that consumes or releases DIC (see details in Aumont et al.[55]), air-sea CO_2 fluxes, and the climatological damping (see supplementary information). Positive values result in a net increase in DIC. All terms were computed online on a daily basis and stored for monthly averages. The DIC tendency (rate of change or trend) equation (Eq. 6) is expressed as a function of monthly anomalies of DIC and fluxes and averaged over the average mixing layer observed during PMHWs in the reanalysis (indicated by angle brackets), i.e. from the surface to h ~ 47 m :

$$\frac{\partial <DIC'>}{\partial t} =< ADV_H' > + < ADV_z' > + < DIFF_z' > + < SBC' > + \frac{<F_{CO2}'>}{h} + < B' > + < r' >. \quad (7)$$

g. Satellite sea surface temperature and marine heatwaves detection

MHWs locations, dates of onset and durations were derived from the global daily remotely sensed National Ocean Atmospheric Administration (NOAA) Optimum Interpolation sea surface temperature V2, ¼° gridded data over 1982-2017[32,33]. This dataset is derived from the advanced very high-resolution radiometer (AVHRR).

We apply a standard MHW detection algorithm[2] to the gridded SST data. In particular, we use 90th percentile threshold criterion and climatology computed from 1983 to 2012. The MHW detection algorithm is usually not performed on grid cells with periods of ice coverage longer than 5 days[10]. We therefore restrict our analysis to the area between 60 °S and 60 °N. For each MHW detected, the date of onset, duration and mean sea surface temperature anomaly are estimated by the MHW detection algorithm.

h. Calculation of anomalies associated with PMHWs

For each PMWH detected, the monthly anomalies were extracted at the model or observation-based products grid-point the closest to the PMHW location and for the entire duration of the PMHW. Then, to match the temporal resolution of the PMHW, the extracted anomalies were resampled from monthly to daily frequency through linear interpolation. The interpolated values were then averaged over the duration of the PMHW to give a single value, consistently with the other metrics derived from the MHW detection algorithm.

5. Data availability

The reanalysis data can be downloaded from the Copernicus Marine Environmental Monitoring Service (https://resources.marine.copernicus.eu/?option=com_csw&view=details&product_id=GLOBAL_ANALYSIS_FORECAST_BIO_001_028). The DIC budget terms data are available upon request from the corresponding author. The BGC-Argo data were downloaded from the Argo Global Data Assembly Centre in France (ftp://ftp.ifremer.fr/argo/). The observation-based product are available from the Surface Ocean pCO2 Mapping Intercomparison website (http://www.bgc-jena.mpg.de/SOCOM/). The SST data are provided by NOAA/ESR/PSL at https://psl.noaa.gov/data/gridded/data.noaa.oisst.v2.highres.html.

6. References

1. Collins, M. *et al.* Extremes, Abrupt Changes and Managing Risk. in *IPCC Special Report on the Ocean and Cryosphere in a Changing Climate* (2019).
2. Hobday, A. J. *et al.* A hierarchical approach to defining marine heatwaves. *Progress in Oceanography* **141**, 227–238 (2016).
3. Holbrook, N. J. *et al.* Keeping pace with marine heatwaves. *Nat Rev Earth Environ* **1**, 482–493 (2020).
4. Bond, N. A., Cronin, M. F., Freeland, H. & Mantua, N. Causes and impacts of the 2014 warm anomaly in the NE Pacific. *Geophys. Res. Lett.* **42**, 3414–3420 (2015).
5. Holbrook, N. J. *et al.* A global assessment of marine heatwaves and their drivers. *Nat Commun* **10**, 1–13 (2019).
6. Lee, T. *et al.* Record warming in the South Pacific and western Antarctica associated with the strong central-Pacific El Niño in 2009-10. *Geophys. Res. Lett.* **37**, (2010).
7. Rodrigues, R. R., Taschetto, A. S., Sen Gupta, A. & Foltz, G. R. Common cause for severe droughts in South America and marine heatwaves in the South Atlantic. *Nat. Geosci.* **12**, 620–626 (2019).
8. Behrens, E., Fernandez, D. & Sutton, P. Meridional Oceanic Heat Transport Influences Marine Heatwaves in the Tasman Sea on Interannual to Decadal Timescales. *Front. Mar. Sci.* **6**, 228 (2019).
9. Frölicher, T. L., Fischer, E. M. & Gruber, N. Marine heatwaves under global warming. *Nature* **560**, 360–364 (2018).
10. Oliver, E. C. J. *et al.* Longer and more frequent marine heatwaves over the past century. *Nat Commun* **9**, 1324 (2018).
11. Smale, D. A. *et al.* Marine heatwaves threaten global biodiversity and the provision of ecosystem services. *Nat. Clim. Chang.* **9**, 306–312 (2019).

12. Laufkötter, C., Zscheischler, J. & Frölicher, T. L. High-impact marine heatwaves attributable to human-induced global warming. *Science* **369**, 1621–1625 (2020).

13. Oliver, E. C. J. Mean warming not variability drives marine heatwave trends. *Clim Dyn* **53**, 1653–1659 (2019).

14. Di Lorenzo, E. & Mantua, N. Multi-year persistence of the 2014/15 North Pacific marine heatwave. *Nature Clim Change* **6**, 1042–1047 (2016).

15. McPhaden, M. J. Genesis and Evolution of the 1997-98 El Nino. *Science* **283**, 950–954 (1999).

16. Oliver, E. C. J. *et al.* The unprecedented 2015/16 Tasman Sea marine heatwave. *Nat Commun* **8**, 16101 (2017).

17. Chen, K., Gawarkiewicz, G. G., Lentz, S. J. & Bane, J. M. Diagnosing the warming of the Northeastern U.S. Coastal Ocean in 2012: A linkage between the atmospheric jet stream variability and ocean response. *J. Geophys. Res. Oceans* **119**, 218–227 (2014).

18. Mills, K. *et al.* Fisheries Management in a Changing Climate: Lessons From the 2012 Ocean Heat Wave in the Northwest Atlantic. *oceanog* **26**, (2013).

19. Ummenhofer, C. C. & Meehl, G. A. Extreme weather and climate events with ecological relevance: a review. *Phil. Trans. R. Soc. B* **372**, 20160135 (2017).

20. Friedlingstein, P. *et al.* Global Carbon Budget 2019. *Earth Syst. Sci. Data* **11**, 1783–1838 (2019).

21. Sabine, C. L. The Oceanic Sink for Anthropogenic CO2. *Science* **305**, 367–371 (2004).

22. Gruber, N. *et al.* The oceanic sink for anthropogenic CO2 from 1994 to 2007. *Science* **363**, 1193–1199 (2019).

23. Ciais, P. *et al.* Carbon and other biogeochemical cycles. in *Climate change 2013: the physical science basis. Contribution of Working Group I to the Fifth Assessment Report of the Intergovernmental Panel on Climate Change* (Cambridge University Press, 2013).

24. Gruber, N. *et al.* Oceanic sources, sinks, and transport of atmospheric CO2. *Global Biogeochem. Cycles* **23**, (2009).

25. Landschützer, P., Gruber, N., Bakker, D. C. E. & Schuster, U. Recent variability of the global ocean carbon sink. *Global Biogeochem. Cycles* **28**, 927–949 (2014).

26. Takahashi, T. *et al.* Climatological mean and decadal change in surface ocean pCO2, and net sea–air CO2 flux over the global oceans. *Deep Sea Research Part II: Topical Studies in Oceanography* **56**, 554–577 (2009).

27. Doney, S. C. *et al.* Mechanisms governing interannual variability in upper-ocean inorganic carbon system and air–sea CO2 fluxes: Physical climate and atmospheric dust. *Deep Sea Research Part II: Topical Studies in Oceanography* **56**, 640–655 (2009).

28. Feely, R. A. *et al.* Seasonal and interannual variability of CO2 in the equatorial Pacific. *Deep Sea Research Part II: Topical Studies in Oceanography* **49**, 2443–2469 (2002).

29. Le Quéré, C., Orr, J. C., Monfray, P., Aumont, O. & Madec, G. Interannual variability of the oceanic sink of CO2 from 1979 through 1997. *Global Biogeochemical Cycles* **14**, 1247–1265 (2000).

30. Liao, E., Resplandy, L., Liu, J. & Bowman, K. Amplification of the ocean carbon sink during El Niños: role of poleward Ekman transport and influence on atmospheric CO_2. *Global Biogeochem. Cycles* (2020) doi:10.1029/2020GB006574.

31. McKinley, G. A., Follows, M. J. & Marshall, J. Mechanisms of air-sea CO2 flux variability in the equatorial Pacific and the North Atlantic. *Global Biogeochem. Cycles* **18**, (2004).

32. Banzon, V., Smith, T. M., Chin, T. M., Liu, C. Y. & Hankins, W. A long-term record of blended satellite and in situ sea-surface temperature for climate monitoring, modeling and environmental studies. (2016).

33. Reynolds, R. W. *et al.* Daily high-resolution-blended analyses for sea surface temperature. *Journal of Climate* **20**, 5473–5496 (2007).
34. Takahashi, T. *et al.* Global sea-air CO2 flux based on climatological surface ocean pCO(2), and seasonal biological and temperature effects. *Deep-Sea Res. Part II-Top. Stud. Oceanogr.* **49**, 1601–1622 (2002).
35. Denvil-Sommer, A., Gehlen, M., Vrac, M. & Mejia, C. LSCE-FFNN-v1: a two-step neural network model for the reconstruction of surface ocean pCO2 over the global ocean. *Geosci. Model Dev.* **12**, 2091–2105 (2019).
36. CMEMS. https://resources.marine.copernicus.eu/?option=com_csw&view=details&product_id=GLOBAL_ANALYSIS_FORECAST_BIO_001_028.
37. Claustre, H., Johnson, K. S. & Takeshita, Y. Observing the Global Ocean with Biogeochemical-Argo. *Annual Review of Marine Science* **12**, (2020).
38. Roemmich, D. *et al.* On the future of Argo: A global, full-depth, multi-disciplinary array. *Frontiers in Marine Science* **6**, 439 (2019).
39. Williams, R. G. & Follows, M. J. *Ocean dynamics and the carbon cycle: Principles and mechanisms*. (Cambridge University Press, 2011).
40. Fennel, K. *et al.* Advancing Marine Biogeochemical and Ecosystem Reanalyses and Forecasts as Tools for Monitoring and Managing Ecosystem Health. *Front. Mar. Sci.* **6**, 89 (2019).
41. Lovenduski, N. S., Gruber, N., Doney, S. C. & Lima, I. D. Enhanced CO2 outgassing in the Southern Ocean from a positive phase of the Southern Annular Mode. *Global Biogeochem. Cycles* **21**, n/a-n/a (2007).

42. Brady, R. X., Lovenduski, N. S., Alexander, M. A., Jacox, M. & Gruber, N. On the role of climate modes in modulating the air–sea CO2 fluxes in eastern boundary upwelling systems. *Biogeosciences* **16**, 329–346 (2019).

43. Ayers, J. M. & Lozier, M. S. Unraveling dynamical controls on the North Pacific carbon sink. *Journal of Geophysical Research: Oceans* **117**, (2012).

44. Landschützer, P., Gruber, N. & Bakker, D. C. Decadal variations and trends of the global ocean carbon sink. *Global Biogeochemical Cycles* **30**, 1396–1417 (2016).

45. Landschützer, P., Gruber, N. & Bakker, D. C. E. An observation-based global monthly gridded sea surface pCO2 product from 1982 onward and its monthly climatology (NCEI Accession 0160558). (2017) doi:10.7289/V5Z899N6.

46. Bakker, D. C. E. *et al.* A multi-decade record of high-quality CO2 data in version 3 of the Surface Ocean CO2 Atlas (SOCAT). *Earth Syst. Sci. Data* **8**, 383–413 (2016).

47. Sabine, C. L. *et al.* Surface Ocean CO2 Atlas (SOCAT) gridded data products. *Earth System Science Data Discussions* **5**, 781–804 (2012).

48. Bakker, D. C. E. *et al.* An update to the Surface Ocean CO2 Atlas (SOCAT version 2). *Earth Syst. Sci. Data* **6**, 69–90 (2014).

49. Pfeil, B. *et al.* A uniform, quality controlled Surface Ocean CO2 Atlas (SOCAT). *Earth Syst. Sci. Data* **5**, 125–143 (2013).

50. Gregor, L., Lebehot, A. D., Kok, S. & Scheel Monteiro, P. M. A comparative assessment of the uncertainties of global surface ocean CO2 estimates using a machine-learning ensemble (CSIR-ML6 version 2019a) – have we hit the wall? *Geosci. Model Dev.* **12**, 5113–5136 (2019).

51. Rödenbeck, C. *et al.* Global surface-ocean pCO2 and sea–air CO2 flux variability from an observation-driven ocean mixed-layer scheme. *Ocean Science* **9**, 193–216 (2013).

52. Iida, Y. *et al.* Trends in pCO2 and sea–air CO2 flux over the global open oceans for the last two decades. *J Oceanogr* **71**, 637–661 (2015).

53. Wanninkhof, R. Relationship between wind speed and gas exchange over the ocean revisited: Gas exchange and wind speed over the ocean. *Limnol. Oceanogr. Methods* **12**, 351–362 (2014).

54. Turi, G., Lachkar, Z. & Gruber, N. Spatiotemporal variability and drivers of pCO2 and air–sea CO2 fluxes in the California Current System: an eddy-resolving modeling study. *Biogeosciences* **11**, 671–690 (2014).

55. Aumont, O., Ethé, C., Tagliabue, A., Bopp, L. & Gehlen, M. PISCES-v2: an ocean biogeochemical model for carbon and ecosystem studies. *Geosci. Model Dev.* **8**, 2465–2513 (2015).

Acknowledgements: This study has been conducted using the Copernicus Marine Service products. The BGC-Argo data were collected and made freely available by the International Argo program and the national programs that contribute to it (https://www.argo.jcommops.org). The Argo program is part of the Global Ocean Observing System.

Authors Contribution: AM, FG, KvS designed the study. AM, KvS wrote the draft of the manuscript, together with FG, PL, CP and SvG. TA and SvG ran the algorithm for the detection of MHWS. JL and CP ran the reanalysis. AM analysed the data. All authors read and approved the final draft.

Competing Financial Interests: The authors declare no competing financial interests.

Materials and correspondence: Correspondence and request for material should be addressed to mignot@mercator-ocean.fr

7. Figures

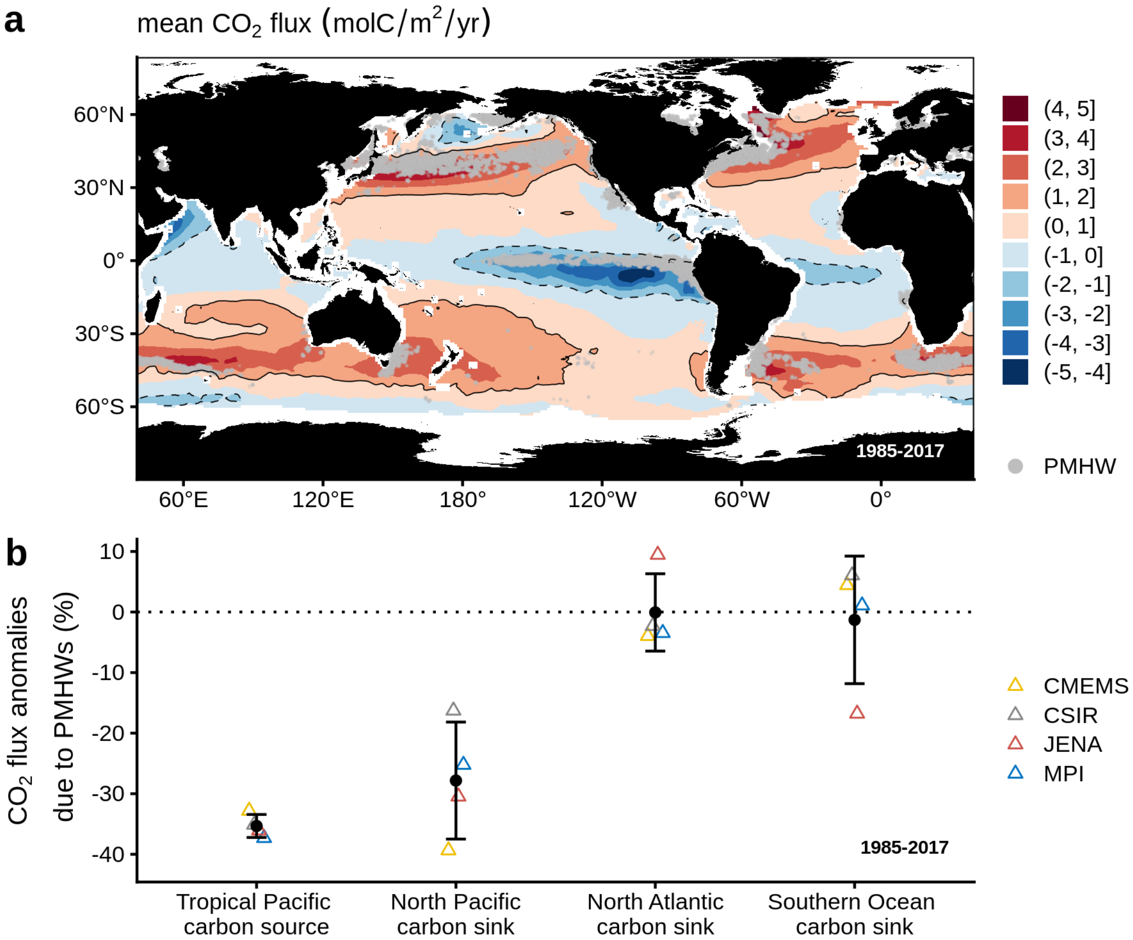

Figure 1. Interplay of PMHWs and oceanic carbon source and sink areas. **(a)** Mean 1985-2017 air-to-sea CO_2 flux (F_{CO2}) derived from the Copernicus Marine Service (CMEMS) observation-based product (see methods section). Positive values indicate oceanic uptake (red), while negative values indicate oceanic outgassing (blue) of CO_2. The black continuous/dashed contours represent critical carbon sink/source regions, i.e the regions where the mean 1985-2017 F_{CO2} is greater/lower than 1/-1 molC/m^2/yr as proposed by Takahashi et al.[34] The grey points represent satellite Sea Surface Temperature grid points that have experienced at least 3 PMHWs from 1985 to 2017 (see text for details). **(b)** Trimmed average percent F_{CO2} anomalies during PMHWs derived from an ensemble of four observation-based products of F_{CO2} (see section methods) in critical oceanic carbon sinks and sources (plain and dashed contours in Fig. 1a) that are impacted by PMHWs. The ensemble mean and standard deviation are given in black. The calculation of the percent F_{CO2} anomalies is detailed in the method section.

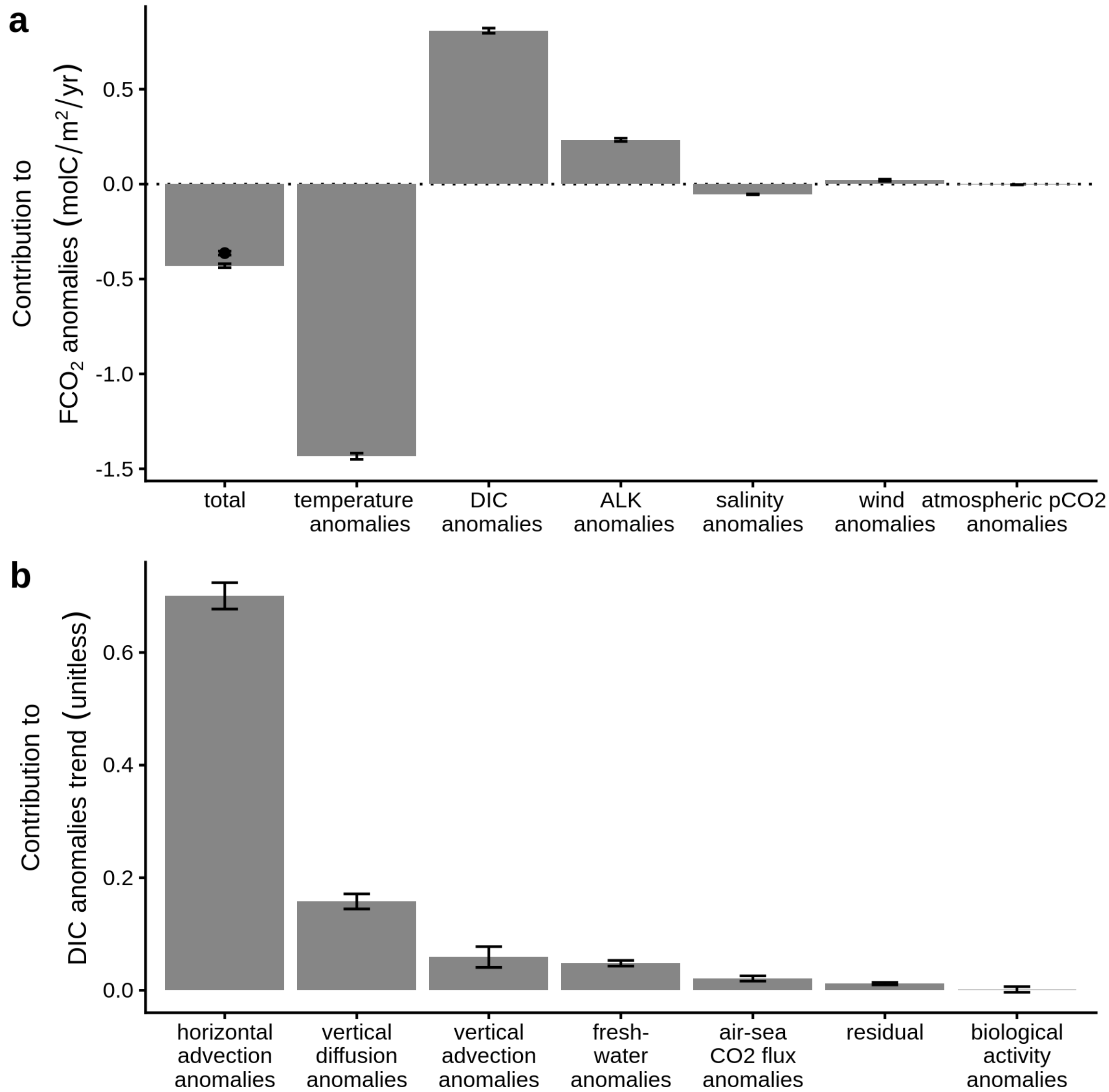

Figure 2. Processes that lead to a reduction in the oceanic uptake of CO_2 in the North Pacific during PMHWs. **(a)** 2009-2017 average F_{CO2} anomalies (black dot) and its Taylor decomposition (vertical bars). The contribution of temperature, Dissolved Inorganic Carbon (DIC), Alkalinity (ALK), salinity, wind and atmospheric partial pressure of CO_2 to F_{CO2} anomalies observed during PMHWs in the North Pacific carbon sink for the 2009-2017 period were calculated using a first order Taylor expansion derived from the biogeochemical reanalysis (see methods section). The “total” bar corresponds to the sum of all contributing terms and corresponds to the Taylor approximation of F_{CO2} anomalies (black dot). The good agreement between the two implies that F_{CO2} anomalies are well approximated by the Taylor decomposition. The error bars correspond to the 95 % confidence interval. **(b)** Contribution of horizontal and vertical advection, vertical diffusion, air-sea flux of CO_2, biological activity, dilution and concentration due to freshwater fluxes and a residual term to the rate of change

(tendency or trend) of DIC anomalies during PMHWs in the North Pacific carbon sink for the 2009-2017 period (see methods section). The vertical bars represent the slope from linearly regressing each forcing term to the DIC anomalies trend[27]. A linear regression slope close to 1 indicates that a particular term produces in-phase anomalies of comparable magnitude. A slope near zero indicates that the term is not important in generating anomalies. The error bars correspond to 95 % confidence intervals.

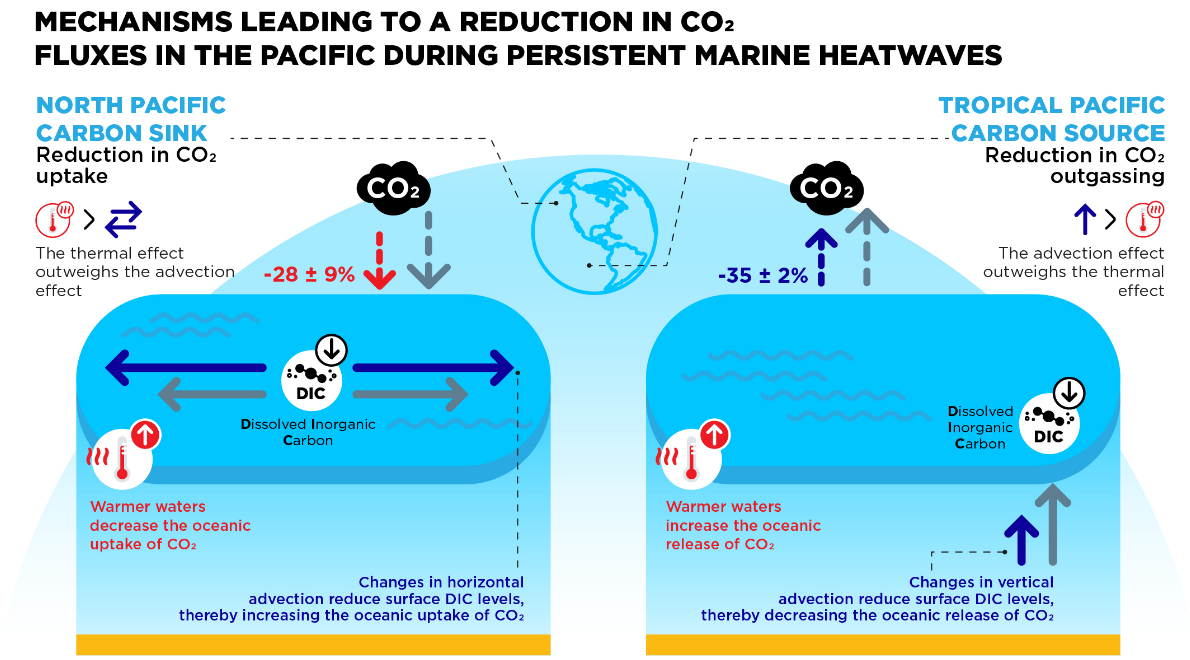

Figure 3. Schematic presentation of the mechanisms driving the reduction in CO_2 fluxes in the Pacific Ocean. Red color indicates the thermal effect on air-sea CO_2 fluxes, the blue color is linked to impacts related to circulations changes associated with PMHWs such as anomalous horizontal and vertical advection. The grey color represents the normal conditions. See text for more details.

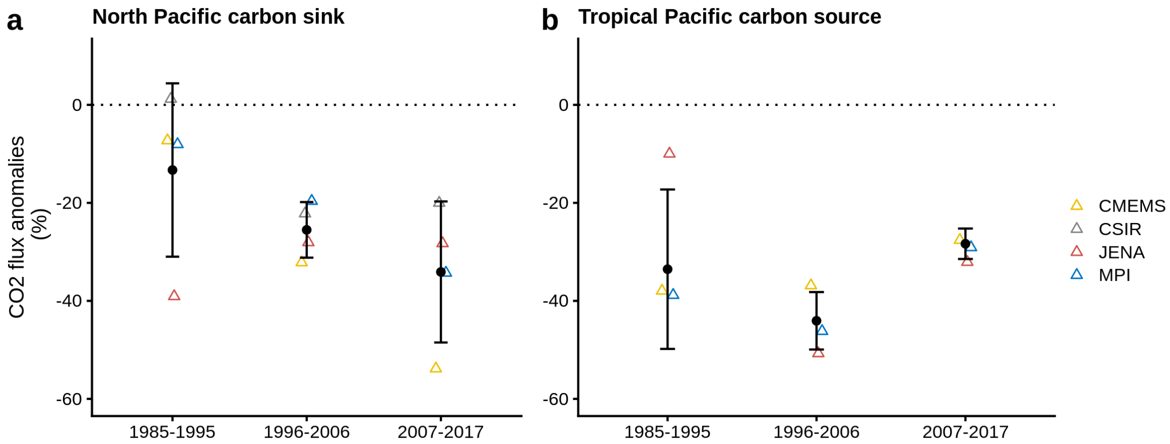

Figure. 4. Evolution of F_{CO2} anomalies due to PMHWs during the 1985-2017 period. Trimmed average percent F_{CO2} anomalies during PMHWs for three time-periods (1985-1995, 1996-2006, 2007-2017) derived from an ensemble of 4 observation-based products of F_{CO2} (see section methods) in the North Pacific carbon sink and in the Tropical Pacific carbon source. The ensemble mean and standard deviation are given in black. The calculation of the percent F_{CO2} anomalies is detailed in the method section.